ACADEMIC PRESS

Available online at www.sciencedirect.com
SCIENCE DIRECT®

Journal of Catalysis 217 (2003) 417–426

JOURNAL OF CATALYSIS

www.elsevier.com/locate/jcat

Sintering of nickel steam-reforming catalysts

Jens Sehested

Haldor Topsøe A/S, Nymøllevej 55, DK-2800 Lyngby, Denmark

Received 18 November 2002; revised 14 February 2003; accepted 17 February 2003

Abstract

Sintering is an important deactivation mechanism for nickel-based steam-reforming catalysts. In this work, the effects of nickel loading, carrier surface area, and temperature on the nickel surface area are studied. The experiments are performed under simulated industrial conditions, i.e., in a mixture of steam and hydrogen (10:1) in the temperature range of 500–682 °C and at 30 bar total pressure. The data are analyzed using a simple model assuming spherical particles and a lognormal metal particle-size distribution with constant standard deviation. It is also assumed that the sintering proceeds via crystallite migration and coalescence. The model predicts well the experimental nickel surface area as a function of nickel loading, carrier surface area, temperature, and time. The model is also used to analyze data from the literature. The model is discussed in the context of predicting metal surface areas of catalysts consisting of small metal particles on ceramic supports.

Keywords: Steam reforming; Prereforming; Nickel catalyst; Sintering; Particle migration

1. Introduction

Sintering is an important deactivation mechanism in many industrial catalysts. A good understanding of the sintering mechanism is crucial, both for predicting the extent of deactivation by this mechanism and for designing catalysts that maintain a high activity. Sintering is a complex process, which may be influenced by many parameters such as temperature, chemical environment, catalyst composition and structure, and support morphology.

An industrial process, for which sintering is important, is steam reforming. In this process hydrocarbons are converted into synthesis gas (CO, CO_2, and H_2):

$$C_nH_m + nH_2O \rightleftarrows nCO + \left(\frac{m}{2} + n\right)H_2,$$

$$CH_4 + H_2O \rightleftarrows CO + 3H_2,$$

$$CO + H_2O \rightleftarrows CO_2 + H_2.$$

Modern steam-reforming units consist of a primary reformer with an adiabatic prereformer upstream, which reduces the load of the primary reformer and minimizes the risk of sulfur poisoning and carbon formation in the primary reformer [1,2]. The primary reformer is operated at 20–40 bar total pressure, high pressures of steam (steam-to-carbon ratio of 1.5–4), and temperatures between 500 and 950 °C. The prereformer is operated adiabatically at 400–550 °C and 20–40 bar total pressure. In both the primary reformer and the prereformer, nickel-based catalysts are commonly used [1].

Nickel steam-reforming catalysts are subject to several deactivation mechanisms during reforming including coking, poisoning, and sintering. Metal particle growth via sintering influences the resistance toward coking and poisoning by sulfur: Coking limits are affected by the nickel particle size [1,2] and the ability for sulfur absorption is related to the nickel surface area [1,2]. Furthermore, the activity depends on the nickel surface area. To predict the performance of an industrial reformer, it is therefore necessary to model the rate of catalyst sintering.

Several studies on the sintering of nickel particles are reported in the literature [1–14]. The most important parameters are the sintering temperature and the atmosphere over the catalyst. Increasing the temperature gives a faster sintering and the presence of water accelerates the sintering process significantly [7]. The initial nickel particle-size distribution, support structure and morphology, and phase transitions of the support are also reported to affect the sintering rate [3,7,8]. Alkali or alkaline-earth promoters on alumina-

E-mail address: JSS@topsoe.dk.

0021-9517/03/$ – see front matter
doi:10.1016/S0021-9517(03)00075-7

supported nickel catalysts have been observed to have a stabilizing effect on the nickel surface area [14]. The effects of poisons such as sulfur in the steam-reforming feed gas are unknown.

It is well established that the rate of loss of metal surface area during sintering of metal particles on a ceramic support is fast at first and then reaches an almost stable level [3–7,10–13]. The loss of metal surface area is well described mathematically by a power-law expression [3,5–7],

$$-\frac{\mathrm{d}A_{\mathrm{Ni}}}{\mathrm{d}t} = kA_{\mathrm{Ni}}^{n}, \tag{1}$$

where A_{Ni} is the nickel surface area as a function of time and k is the decay rate constant. The experimentally established values of n are generally 7 or higher, at least for temperatures up to 700 °C [7]. It should be noted that 2 must to be added to the values of n reported in [7] to get the n value used here.

The aim of this work is to study the behavior of the nickel surface area of supported catalysts during sintering and investigate the effects of nickel loading, support area, and temperature. In this work, a simple model, which describes the surface area of nickel catalysts supported on a ceramic support as a function of the total surface area, the nickel loading, the temperature, and the time, is presented. The model is tested against the data obtained here and selected literature data.

2. Experimental

Eight experimental steam-reforming catalysts were used in the sintering experiments reported here. The catalysts were prepared using three different supports: catalyst 1 containing 22 wt% Ni was supported on a 24 m^2/g (BET area) $MgAl_2O_4$ spinel support; catalysts 2–4 consisted of a 15 m^2/g (BET area) $MgAl_2O_4$ spinel support to which was added 16.5, 19.3, and 23.1 wt% Ni; and catalysts 5–8 were supported on a 50 m^2/g (BET area) Zr-doped $MgAl_2O_4$ spinel support containing 8, 15, 25, and 30 wt% Ni. The catalysts were reduced in H_2 at 500 °C for 2 h and passivated overnight immediately after reduction at 50 °C in a mixture of 1 v/v% air in N_2 followed by 2 h in 1 v/v% O_2 in N_2 before they were removed from the reactor. Prior to sintering, the catalysts were reactivated by reduction in H_2 at 500 °C for 2 h.

Two sets of sintering experiments were performed. In the first set of experiments, all catalysts were sintered isothermally. In the second set of experiments samples of catalyst 1 were sintered at various temperatures in the temperature range of 520–682 °C. The detailed sintering conditions are given in Table 1.

The experimental setup used for these experiments was operated at a total pressure of 30 bar and at high partial pressures of steam. All the parts of the system with high partial pressures of steam could be heated. The temperature of the gas in the catalyst bed was measured by a movable thermocouple in a small tube through the center of the reactor. The diameter and the length of the reactor are approximately 4 and 100 cm, respectively. The catalyst samples were kept in small stainless-steel nets. The bottom of the nets covered the cross section of the reactor and fitted over the internal tube in the reactor. The catalyst samples were situated at the bottom of the nets. The length of the part of the reactor containing nets was 25–30 cm.

Table 1
Sintering conditions

Catalyst number	H_2O:H_2	Total pressure	Temperature	Time
2–4	10:1	30 bar	500 °C	664 h
1, 5–8	10:1	30 bar	500 °C	700 h
1	10:1	30 bar	520–682 °C	700 h

The surface areas (BET) of some of the catalysts were determined by nitrogen adsorption using a Quantachrome MONOSORB apparatus. The measured values were normalized to standard temperature and pressure in accordance with the ASTM standard for a single-point determination of the BET surface areas [15]. The surface area of the internal standard was measured daily giving a standard deviation of less than 2%.

The sulfur chemisorption capacity was used to obtain the nickel surface area relative to a reference sample from which a relative surface-averaged nickel-particle diameter can be derived. Chemisorption of sulfur was carried out in a separate reactor according to Rostrup-Nielsen and coworkers [1,2] using a mixture of H_2S/H_2 until saturation. Under these experimental conditions, the Ni surface area is proportional to the sulfur capacity. The sulfur uptake of a catalyst was determined by oxidation of chemisorbed sulfur at high temperature and the amount of SO_2 that is liberated was measured by infrared detection. The chemisorption of sulfur is discussed in more detail by Alstrup et al. [16].

The nickel surface areas obtained by this method have recently been compared to those acquired by hydrogen chemisorption [2] and anomalous small angle X-ray scattering (ASAXS) [13]. Hydrogen and sulfur chemisorption gives approximately the same active surface areas. The nickel surface areas determined by ASAXS and sulfur chemisorption are proportional, but ASAXS gives slightly higher surface areas probably because parts of the nickel crystallites cannot be probed by sulfur (or hydrogen) due to wetting of the support by nickel.

The relative nickel surface area, A_{Ni}, is converted to a relative surface-averaged nickel particle diameter, $\bar{d}_{\mathrm{s}}$, by [1]

$$\bar{d}_{\mathrm{s}} = \mathrm{const.}\frac{X_{\mathrm{Ni}}}{A_{\mathrm{Ni}}}, \tag{2}$$

where X_{Ni} is the fractional nickel loading (Ni wt%/100).

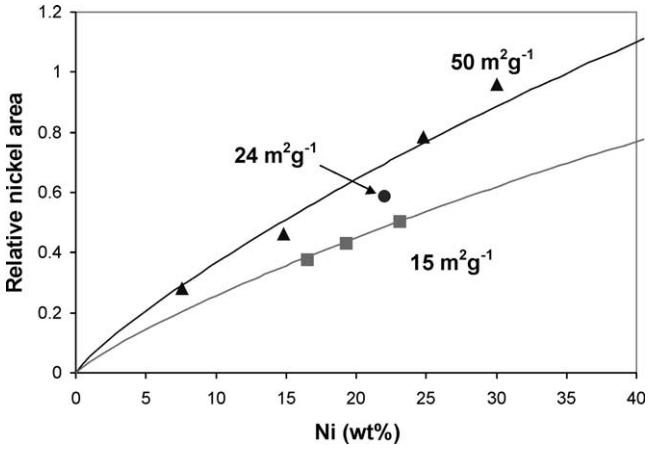

Fig. 1. Relative nickel surface areas after long sintering times (> 600 h) of catalysts supported on $MgAl_2O_4$ with various surface areas plotted as a function of the nickel wt%. The sintering conditions were 500 °C, H_2O:H_2 = 10:1, and 30 bar total pressure. The lines are fitted to the data using Eq. (25). See text for details.

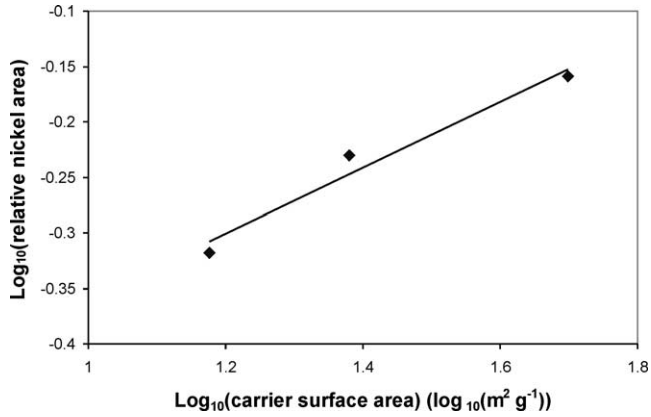

Fig. 2. Log_{10} of the relative nickel surface areas at 22 wt% nickel after long sintering times (> 600 h) of catalysts supported on $MgAl_2O_4$ plotted as a function of log_{10} of the surface area of the carrier. The sintering conditions were 500 °C, H_2O:H_2 = 10:1, and 30 bar total pressure. The data points for the 50 and 15 $m^2\,g^{-1}$ carriers were obtained by interpolation. See text for details.

3. Results

In the following, the results obtained in the two sets of sintering experiments are given. The first set of experiments was performed to determine the dependence of the nickel surface area on the support area and nickel loading. Catalysts 1–8 were studied and the relative nickel surface areas obtained after 664 h (catalysts 2–4) and 700 h (catalysts 1, 5–8) of sintering are plotted in Fig. 1. Since the loss rate of the nickel surface area after 664 h of sintering is low, there is no correction applied for this difference in sintering time. Using the time dependence of the nickel surface area in the model derived below, the loss of surface area of catalysts 2–4 from 664 to 700 h is calculated to be 2%. It therefore seems reasonable to neglect this factor in the following.

The data in Fig. 1 show that the nickel loading and the carrier surface area affect the nickel surface area after sintering. In Fig. 2, the relative nickel surface area after sintering is plotted as a function of the area of the carrier at 22 wt% Ni. The data in Fig. 2 for the 50 $m^2\,g^{-1}$ and the 15 $m^2\,g^{-1}$ carriers were obtained by linear interpolation of the two data points with higher and lower nickel loading than 22 wt% Ni. It can be concluded from Fig. 2 that the nickel surface area, A_{Ni}, after sintering depends only weakly on the surface area of the carrier, A_{car}, namely by the carrier surface area in the order of 0.3 ± 0.1. The reason for this rather surprisingly weak dependence of A_{Ni} on A_{car} can be understood when the sintering is assumed to proceed via particle migration and coalescence as discussed in detail below.

The dependence of the nickel surface area on the temperature was studied in the second set of experiments. Seven samples of catalyst 1 were placed at different positions from the top to the bottom of the reactor and heated in 30 bar of N_2 to a temperature of about 450 °C at the entrance and about 650 °C at the exit of the catalyst bed. After the temperature was stabilized, hydrogen and then steam were allowed into the reactor such that a H_2O:H_2 ratio of 10:1 was obtained and the flow of nitrogen was switched off. The temperature was then increased to reach the desired temperature range of 500–700 °C. The temperature at the position of each catalyst sample was carefully measured using the movable thermocouple inside the inner tube of the reactor. These conditions were kept constant for 700 h. After shutdown, the relative nickel surface areas of the catalyst after 700 h of sintering were determined by sulfur chemisorption. The data are plotted in Fig. 3 as a function of $1000/RT$ where T(K) is the temperature at the position of the catalyst sample. As seen from this figure, the temperature is a very important parameter for the nickel surface areas of aged catalysts. In addition, the logarithm of the nickel surface areas depends almost linearly on $1000/RT$ and the data are analyzed by an Arrhenius type expression,

$$A_{Ni}(T) = A_{Ni}^{\infty} e^{-E_a/RT}, \tag{3}$$

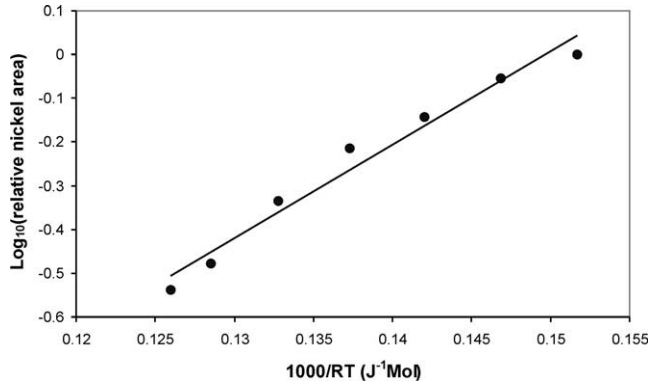

Fig. 3. Log_{10} of the relative nickel surface areas of catalysts containing 22 wt% nickel supported on a 24 $m^2\,g^{-1}$ $MgAl_2O_4$ carrier plotted as a function of the measured temperature at the position of the catalyst sample. The catalysts were sintered for 700 h in an atmosphere with a steam to hydrogen ratio of 10:1 and 30 bar total pressure. The line is a fit of an Arrhenius type expression to the experimental data. See text for details.

where $A_{Ni}(T)$ is the nickel surface area as a function of the temperature after 700 h of sintering, A_{Ni}^{∞} is the nickel surface area at $T = \infty$ after 700 h of sintering, and E_a is the apparent Arrhenius energy for the loss of nickel surface area of the used catalysts. A value for this Arrhenius energy of -49 ± 7 kJ/mol is obtained. This Arrhenius energy is related to the activation energy for diffusion of nickel atoms and the concentration of "free" nickel add-atoms on the surface of the nickel particles as discussed below. The BET areas of the catalyst sintered at the highest and the lowest temperatures were measured and the loss of surface area during sintering was determined to be 43 and 17%, respectively. This loss of surface area may be caused by loss of carrier surface area as well as nickel surface area. If it is assumed that the loss in BET area is due to a decrease in the surface area of the carrier and that the BET areas of the catalyst samples at intermediate temperatures can be determined by interpolation using an expression analogous to expression [3], $A_{BET}(T) = A_{BET}^{\infty} e^{-E_a/RT}$, then the it is possible to correct the data in Fig. 3. The nickel surface areas, $A_{Ni,\,corrected}$, the samples would have had if the BET areas were stable, are obtained from the observed nickel surface area, $A_{Ni,\,observed}$, by the following expression:

$$\frac{A_{Ni,\,corrected}}{A_{Ni,\,observed}} = \left(\frac{A_{BET}(fresh)}{A_{BET}(T)}\right)^{n}. \quad (4)$$

Using $n = 0.3$ as found experimentally above an apparent Arrhenius energy for the plot in Fig. 3 of -45 kJ/mol is derived. If the theoretical value of $n = 0.14$ determined later is used, then the Arrhenius energy for the plot in Fig. 3 is -47 kJ/mol. From these values, an apparent Arrhenius energy of -46 ± 8 kJ/mol for the plot in Fig. 3 is reported.

4. Discussion

In this section, a simple model is derived describing the metal surface area of supported catalysts as a function of time, temperature, surface area of the carrier, and nickel loading. Four assumptions will be made to simplify the very complex problem of sintering of metal particles on ceramic supports. The four assumptions include: (i) the particle size distribution (PSD) of the metal particles is lognormal; (ii) the sintering mechanism is particle migration and coalescence; (iii) the effect of the carrier is only to separate the metal particles; and (iv) the average metal particle diameter can be used to describe the sintering of the metal particles. These assumptions are discussed in detail below. Finally, the predictions of the model are compared with the experimental data obtained in this work and with selected data from the literature.

4.1. Particle-size distribution

It is assumed in the following that the metal particle-size distribution is lognormal. Several authors have studied metal particle size distributions [2–6,10–13,17–20] and observed that metal particle sizes are in most cases lognormally distributed after sintering at moderate temperatures (about $< 700\,^{\circ}C$) [2–5,10,13,17–20]. The standard deviation of the lognormal PSDs were found to be 1.32 ± 0.12 and independent of time [20]. The rate of sintering at a given set of experimental conditions depends on the initial metal particle size distribution as discussed by Richardson and Crump [3] and Wanke [21]. It may prove difficult to obtain the PSD for the fresh catalyst with sufficient precision to calculate the initial rate of sintering and quantitative comparisons of the time development of the metal areas or the average metal particle diameters of different catalysts reported in the literature. For some catalysts, especially catalysts with low metal loading under mild sintering conditions, the sintering is slow and almost constant. In this case, the initial sintering, which depends on the properties of the fresh catalyst, is obviously crucial. These complications may make a fundamental understanding of the phenomena of sintering difficult. Fortunately, lognormal PSDs are often developed after a period of sintering and the sintering proceeds with this distribution but with increasing average diameter. In some cases the particle sizes are lognormally distributed already at the beginning of the sintering experiment [4,5,10,13,17–20]. With lognormal PSDs with constant standard deviation, the sintering is fully described by an average metal particle size or the metal area and this will be used to obtain the model below.

4.2. Sintering mechanism

Generally, two mechanisms are proposed for the sintering of metal particles on ceramic supports: atom migration (Ostwald ripening) and particle migration (coalescence). Ostwald ripening refers to the process where metal atoms are emitted from one metal particle and captured by another metal particle. In the coalescence process, the particles themselves move over the support and collide to form larger particles. The driving force for both processes is the surface energy. In both these processes, sintering slows down with time.

According to Granqvist and Buhrman [17–20] and Wynblatt and Gjostein [22], Ostwald ripening results in a particle-size distribution, which has a tail toward the small particles and a steep slope toward the larger particle sizes. A recent computer simulation [23] confirms these characteristics of the size distribution from Ostwald ripening. However, Fuentes and Salinas-Rodriguez [24] recently found that mathematically under certain conditions, Ostwald ripening also gives rise to PSDs that look similar to lognormal distributions casting some doubt on whether the particle-size distribution can be used to discriminate between various sintering mechanisms. However, further work is needed to verify that Ostwald ripening results in particle-size distributions, which look lognormal, when reasonable physical parameters are chosen.

It is interesting to compare the measurements of particle-size distributions done together with measurements of the nickel surface area as a function of time. The surface area as a function of time, A_{Ni}, may be fitted by a *power law expression* [3,5–7,13,25], Eq. (1). As previously discussed the experimentally observed powers of $A_{\mathrm{Ni}}(n)$ are generally 7 or higher at least for temperatures up to 700 °C [7,25] when the samples are kept in their reduced state. When the particle-size distributions and the decay kinetics of the surface area were measured simultaneously, lognormal particle-size distributions were found and n ($\geqslant 8$) which indicates that particle migration and coalescence are responsible for sintering in these cases [3,5,6,13].

At higher temperatures (> 700 °C), other particle-size distributions are observed and with lower values of n in Eq. (1) pointing toward another sintering mechanism [5,6,13]. Lower values of n indicate that atomic migration is the dominant sintering mechanism [22,25] supporting the conclusions of earlier theoretical work that atomic migration gives rise to particle-size distributions with a tail toward the small particle sizes and an abrupt cutoff at large particle diameters.

Support for the view that the particle migration and coalescence sintering mechanism are dominating at moderate temperatures was reported recently [26]. Hansen et al. [26] observed migration and coalescence of ruthenium particles at a BN (boron nitride) support at 500 °C using in situ electron microscopy. Energy considerations also support the conclusion that particle migration and coalescence are dominating sintering at moderate temperatures while atomic migration is the sintering mechanism at high temperatures. The energy required to move a metal atom from a metal particle to the surface of the support is high—about the same as the heat of sublimation of metals [25], for example, 427 kJ mol^{-1} for Ni [27]—while the adsorption of metal atoms on ceramic carriers is generally assumed to be of the van der Waals type and therefore small [25]. The activation energy for sintering via atomic migration in steam reforming may decrease by nickel atoms binding to absorbants such as oxygen atoms or OH radicals. However, the formation energy of, for example, nickel add-atoms on a nickel surface (Ni(111)) is only of the order of 111 kJ/mol [28] which is apparently much lower than that of the formation of metal atoms on a carrier as discussed above. Even with a significant stabilization of the metal atoms on the carrier by absorbants, impurities, or defects, it is still expected that the activation energy for the atomic migration mechanism is much higher than for particle migration and coalescence.

In conclusion, the experimental data suggest that particle migration and coalescence is the main sintering mechanism at low temperatures (< 700 °C for Ni) while atomic migration is the dominant sintering mechanism at high temperatures. It should also be noted that since $n_{\text{particle migration}} > n_{\text{Ostwald ripening}}$ in Eq. (1), Ostwald ripening will be relatively more important after longer periods of sintering. In the model derived below, sintering is for reasons of simplicity assumed to proceed via particle migration and coalescence and particle migration is taken as the rate-determining step as opposed to the coalescence process.

4.3. Carrier

In the following, the carrier is considered only as a surface with a certain surface area where the metal particles are situated. This means that the bindings between the carrier and the metal particles are weak and have no influence on the metal PSDs. The interaction between the carrier and metal particles has been discussed by Wynblatt and Gjostein [22] and Hughes [25]. Wetting of the support by the metal reduces sintering but most pure metal-ceramic substrate systems show only a weak wetting [29] with contact angles around 80–100°. For simplicity the metal particles are assumed to be spherical in the following. However, it should be noted that adsorbants in some chemical systems have a significant impact on the ability of metallic particles to wet a support as observed for the Cu/ZnO system [30].

The pore structure and the morphology of the carrier will be ignored. It is therefore assumed that the metal particles can always find room for development. This assumption is supported by the recent work by Sehested et al. [10] who have found that the mobility of the metal particles determined their size in the sintered catalyst rather than the pore size. However, it should be noted that Richardson and coworkers [3,11] found a significant effect of the pore system on sintering, and sintering models that take the pore structure of the carrier into account have been published [31–33].

4.4. Average particle diameter

Finally, it is assumed that it is possible to use the average particle diameter to describe the changes of the PSD. This hypothesis is built on the previous assumption that the PSDs are lognormal and that the standard deviations of the distributions are constant. It has been reported that the PSD keeps its lognormal shape during sintering [10,13,17–20]. Granqvist and Buhrman [20] determined the standard deviation of the lognormal PSDs to be 1.32 ± 0.12. The following integrals over lognormal PSDs of the particle diameter in the power of n, $\langle d^n \rangle$, are helpful in the derivation of the model.

$$\begin{aligned}\langle d^n \rangle &= \int_{-\infty}^{\infty} d^n f_{\mathrm{LN}}(d)\,\mathrm{d}\left(\ln\frac{d}{\bar{d}}\right)\\ &= \frac{\bar{d}^n}{(2\pi)^{0.5}\ln(\sigma)}\int_{-\infty}^{\infty}\left(\exp\left(\ln\frac{d}{\bar{d}}\right)\right)^n\\ &\quad\times\exp\left(-\frac{1}{2\ln^2(\sigma)}\left(\ln\frac{d}{\bar{d}}\right)^2\right)\mathrm{d}\left(\ln\frac{d}{\bar{d}}\right) = a\bar{d}^n, \qquad (5)\end{aligned}$$

where $\bar{d}$ is the number averaged particle diameter; σ is the standard deviation of the lognormal distribution;

$$f_{\mathrm{LN}}(d) = \frac{1}{(2\pi)^{0.5}\ln(\sigma)}\exp\left(-0.5\left(\frac{\ln(d/\bar{d})}{\ln(\sigma)}\right)^2\right)$$

is the number of particles dn in a logarithmic size interval $\mathrm{d}(\ln(d))$; and $a = \exp(0.5n^2\ln^2(\sigma))$ is a constant dependent on n. Hence, the integrals over lognormal PSDs of functions proportional to the particle diameter in the power of n, $\langle d^n\rangle$ equal the average diameter in the power of n times a constant. For example, the surface averaged diameter and the total volume of the metal particles are calculated by

$$\bar{d}_{\mathrm{surface}} = \frac{\langle d^3\rangle}{\langle d^2\rangle} = \frac{\exp\left(\frac{9}{2}\ln^2(\sigma)\right)\bar{d}^3}{\exp\left(\frac{4}{2}\ln^2(\sigma)\right)\bar{d}^2} = \exp\left(\frac{5}{2}\ln^2(\sigma)\right)\bar{d} \approx 1.21\bar{d}, \tag{6}$$

$$V_{\mathrm{p}} = \frac{\pi}{6}\langle d^3\rangle = \frac{\pi}{6}\exp\left(\frac{9}{2}\ln^2(\sigma)\right)\bar{d}^3 \approx 0.74\bar{d}^3, \tag{7}$$

when $\sigma = 1.32$.

4.5. Derivation of model

With these simplifications, the model for the time development of the average metal particle diameter and the metal area is derived. Following Ruckenstein and Pulvermacher [34], the rate of collision, $\mathrm{d}\Phi_j(s^{-1})$, of a particle j with a diameter of d_j with particles k with a diameter d_k in the logarithmic size interval $\mathrm{d}\ln(d_k)$ is given by

$$\mathrm{d}\Phi_j = \text{const.}D_{kj}\,\mathrm{d}c_k = \text{const.}D_{kj}c_{\mathrm{car}}f_{\mathrm{LN}}(d_k)\,\mathrm{d}\ln(d_k), \tag{8}$$

where c_{car} is the total number of metal particles per square meter of the carrier and D_{kj} is the relative diffusion constant for particles of diameters d_k and d_j:

$$D_{kj} = D_k + D_j. \tag{9}$$

$\mathrm{d}c_k$ is the number of particles per square meter of diameter d_k in the diameter interval $\mathrm{d}\ln(d_k)$, and "const." will be used in the following as an arbitrary constant, which may vary from equation to equation.

Uncertainty exists of whether $\mathrm{d}\Phi_j$ can be considered proportional to $D_{kj}\,\mathrm{d}c_k$. Ruckenstein and Pulvermacher [34] were not able to derive a time-independent expression of "const." in two dimensions. They had to introduce a second time scale denoted θ which was short compared to the sintering time t. Ruckenstein and Pulvermacher considered the parameter $D_{kj}\theta/R_{kj}^2$, where $R_{kj} = r_k + r_j$ is the sum of the particle radii. They found that when $D_{kj}\theta/R_{kj}^2 \gg 1$, "const." in Eq. (8) is nearly a time-independent constant. This is the case when θ is chosen to be so large that $D_{ij}\theta/R_{ij}^2 \gg 1$ and so small that θ fulfills the condition $\theta \ll t$. Interestingly, Chandrasekhar [35] obtained an expression for Φ in three dimensions which is independent of time as long as the distance between the particles is much longer than the radii of the particles. Here, "const." is assumed to be a time-independent constant.

If X_{Me} is the fractional mass of metal in gram metal per gram of catalyst, then the number of particles per gram catalyst, c_{cat}, is given by

$$c_{\mathrm{cat}} = \text{const.}\frac{X_{\mathrm{Me}}}{\rho_{\mathrm{Me}}\bar{d}^3}, \tag{10}$$

where $\bar{d}$ is the average particle diameter and ρ_{Me} is the density of the metal. The number of particles per square meter of the carrier, c_{car}, may be obtained from

$$c_{\mathrm{car}} = \text{const.}\frac{X_{\mathrm{Me}}}{\rho_{\mathrm{Me}}(1 - X_{\mathrm{Me}})A_{\mathrm{car}}\bar{d}^3}, \tag{11}$$

where A_{car} is the surface area of the carrier per gram of the carrier. Making the integration of Eq. (8) over the k particles, an equation for Φ_j is obtained assuming that the diffusion constant, D_{kj}, is a sum of two functions that are proportional to d_k^n and d_j^n, respectively, $D_{kj} = D(d_k^n) + D(d_j^n)$,

$$\Phi_j\ \left(\mathrm{s}^{-1}\right) = \text{const.}c_{\mathrm{car}}\int_{-\infty}^{\infty} D_{kj}f_{\mathrm{LN}}(d_k)\,\mathrm{d}\ln\left(\frac{d_k}{\bar{d}}\right) = \text{const.}c_{\mathrm{car}}\left(D\left(d_j^n\right) + D\left(\bar{d}^n\right)\right), \tag{12}$$

where Φ_j is the rate of collision of a particle j with a diameter d_j. The total number of particle collisions per gram of catalyst, Φ ($\mathrm{s}^{-1}\,\mathrm{g}^{-1}$), may be calculated from Eq. (13)

$$\Phi\ \left(\mathrm{s}^{-1}\,\mathrm{g}^{-1}\right) = c_{\mathrm{cat}}\int_{-\infty}^{\infty}\Phi_j\left(s^{-1}\right)f_{\mathrm{LN}}(d_j)\,\mathrm{d}\ln\left(\frac{d_j}{\bar{d}}\right) = \text{const.}c_{\mathrm{cat}}c_{\mathrm{car}}D\left(\bar{d}^n\right). \tag{13}$$

If two particles of diameters d_j and d_k collide and coagulate, the resulting particle will have a diameter of $(d_j^3 + d_k^3)^{1/3}$. The average increase in the average diameter for one collision in N particles is obtained from

$$\begin{aligned}\Delta(\bar{d}) &= \int_{-\infty}^{\infty}\int_{-\infty}^{\infty}\left(\frac{(N\bar{d} - d_j - d_k + (d_k^3 + d_j^3)^{1/3}}{N-1} - \bar{d}\right) \times f_{\mathrm{LN}}(d_j)\,\mathrm{d}\left(\ln\frac{d_j}{\bar{d}}\right)f_{\mathrm{LN}}(d_k)\,\mathrm{d}\left(\ln\frac{d_k}{\bar{d}}\right)\\ &= \int_{-\infty}^{\infty}\int_{-\infty}^{\infty}\left(\frac{(N-2)\bar{d} + (d_k^3 + d_j^3)^{1/3}}{N-1} - \bar{d}\right)f_{\mathrm{LN}}(d_j) \times \mathrm{d}\left(\ln\frac{d_j}{\bar{d}}\right)f_{\mathrm{LN}}(d_k)\,\mathrm{d}\left(\ln\frac{d_k}{\bar{d}}\right)\\ &= \int_{-\infty}^{\infty}\int_{-\infty}^{\infty}\left(\frac{(d_k^3 + d_j^3)^{1/3} - \bar{d}}{N-1}\right)f_{\mathrm{LN}}(d_j) \times \mathrm{d}\left(\ln\frac{d_j}{\bar{d}}\right)f_{\mathrm{LN}}(d_k)\,\mathrm{d}\left(\ln\frac{d_k}{\bar{d}}\right)\end{aligned}$$

$$= \frac{\bar{d}}{N-1} \int_{-\infty}^{\infty} \int_{-\infty}^{\infty} \left(\left(\frac{d_k^3}{\bar{d}^3} + \frac{d_j^3}{\bar{d}^3} \right)^{1/3} - 1 \right) f_{\mathrm{LN}}(d_j) \times \mathrm{d}\left(\ln \frac{d_j}{\bar{d}} \right) f_{\mathrm{LN}}(d_k)\, \mathrm{d}\left(\ln \frac{d_k}{\bar{d}} \right). \quad (14)$$

The integrals have been solved by numerical integration and it can be shown that they are equal to a constant independent of $\bar{d}$. Hence, the increase in the average diameter per collision, $\Delta\bar{d}$, in a large number of particles, N, is given by

$$\Delta(\bar{d}) = \text{const.} \frac{\bar{d}}{N-1} \approx \text{const.} \frac{\bar{d}}{N}. \quad (15)$$

The average increase in the average particle diameter after one particle collision in 1 g of catalyst is obtained by substitution of N by c_{cat} in Eq. (15). The unit of $\Delta\bar{d}$ is in this case (g m). Using Eqs. (13) and (15), it is now possible to calculate the increase in particle average diameter as a function of time per gram of catalyst:

$$\frac{\mathrm{d}(\bar{d})}{\mathrm{d}t} = \Phi\,\Delta(\bar{d}) = \text{const.} \frac{\bar{d}}{c_{\mathrm{cat}}} c_{\mathrm{cat}} c_{\mathrm{car}} D\left(\bar{d}^n\right) = \text{const.} \frac{D(\bar{d}^n) X_{\mathrm{Me}}}{\rho_{\mathrm{Me}}(1 - X_{\mathrm{Me}}) A_{\mathrm{car}} \bar{d}^2}. \quad (16)$$

If $D(\bar{d}^n)$ is known, an expression for $(\mathrm{d}(\bar{d}))/\mathrm{d}t$ can be derived. According to Gruber [36], the diffusion coefficient for spherical metal particles, $D_{\mathrm{p}}^{\mathrm{spherical}}$, is related to the diffusion coefficient for metal atoms on the particle surface, D, by

$$D_{\mathrm{p}}^{\mathrm{spherical}} = 4.818 D \left(\frac{a_0}{d} \right)^4, \quad (17)$$

where d is the diameter of the metal particle and a_0 is the atomic diameter of the metal, which for nickel is 2.3 Å. In the following, the discussion will be concentrated on nickel particles on a ceramic support.

Eq. (17) is true in an inert atmosphere and if all surface atoms contribute to the mass transport at the surface of the particle. However, in an atmosphere, which does not interact with the surface, add-atoms are expected to dominate the surface transport. The diffusion constant for spherical particles, when add-atoms are responsible for the mass transport at the particle surface, is given by

$$D_{\mathrm{particle}}^{\text{add-atom}} = 4.818 D_{\text{add-atom}} \left(\frac{a_0^4}{d^4} \right) K_1, \quad (18)$$

where $D_{\text{add-atom}}$ is the diffusion coefficient of an add-atom on a nickel surface and K_1 is the equilibrium constant for the following reaction:

$$\mathrm{Ni}(111) + \mathrm{Ni}_{\mathrm{bulk}} \rightleftharpoons \text{Ni add-atom on Ni}(111). \quad (19)$$

Hence, K_1 is given by

$$K_1 = \frac{\theta_{\text{add-atom}}}{1 - \theta_{\text{add-atom}}}, \quad (20)$$

where $\theta_{\text{add-atom}}$ is the coverage of add-atoms at a Ni(111) surface. According to Bengaard [28], K_1 is activated by approximately 111 kJ/mol and this energy contributes to the overall activation energy of the sintering process.

In atmospheres that do interact with the nickel surface, the equilibrium between gas-phase species and surface species may change the energies of metal add-species, thereby changing the abundance and the mobility of the species responsible for the mass transport at the surface of the metal particles. Adsorption of OH to a nickel dimer in a Ni(111) surface reduces the energy of formation by ca. 87 kJ mol^{-1} [28]. This species may therefore be much more abundant at the surface on the nickel particles than nickel add-atoms when high pressures of steam are present in the atmosphere over the catalyst. Another example of the importance of the atmosphere over a supported catalyst was published by Handa and Matthews [37]. These authors studied the sintering of Pt particles on Al_2O_3 in the presence of He, H_2, and O_2 experimentally and theoretically. The behavior in an O_2 atmosphere as compared to in a H_2 atmosphere was described by rapid loss of Pt atoms from the Pt particles, slow transport at the surface of the carrier, and low probability of incorporation of Pt atoms into the Pt particles. It is clear from these examples that the atmosphere has a very important effect on the rate of sintering. However, it is not within the scope of this paper to go into detail regarding the influence of the atmosphere on the rate of sintering.

For spherical particles and with add-atoms as the dominating mass transport species at the particle surface, $D = D_{\text{particle, Ni}}^{\text{spherical, add-atom}}$ can be introduced into Eq. (16) to obtain an expression for $(\mathrm{d}(\bar{d}_{\mathrm{Ni}}))/\mathrm{d}t$,

$$\frac{\mathrm{d}(\bar{d}_{\mathrm{Ni}})}{\mathrm{d}t} = \text{const.} \frac{D_{\mathrm{Ni}} X_{\mathrm{Ni}}}{(1 - X_{\mathrm{Ni}}) A_{\mathrm{car}} \bar{d}_{\mathrm{Ni}}^6} K_1, \quad (21)$$

where ρ_{Ni} and a_0 are included in the constant. It is interesting to compare the dependence of $(\mathrm{d}(\bar{d}_{\mathrm{Ni}}))/\mathrm{d}t$ on $\bar{d}_{\mathrm{Ni}}$, obtained from Eq. (21), to the results reported by Wymblatt and Gjostein [22] and Ruckenstein and Pulvermacher [34]. By numerical integration of particle-size distributions, Ruckenstein and Pulvermacher found kinetic expressions for the sintering process. There authors found that if the diffusion coefficient for the metal particles depends on $\bar{d}_{\mathrm{Ni}}$ in the power of $-p$ then $(\mathrm{d}(\bar{d}_{\mathrm{Ni}}))/\mathrm{d}t$ depends on $\bar{d}_{\mathrm{Ni}}$ in the power of $-p-2$. Hence, if D_{Ni} is proportional to $\bar{d}_{\mathrm{Ni}}^{-4}$, the numerical solutions including the particle-size distribution performed by Ruckenstein and Pulvermacher [34] predict that $(\mathrm{d}(\bar{d}_{\mathrm{Ni}}))/\mathrm{d}t$ is proportional to $\bar{d}^{-6}$. This is the same dependence of $(\mathrm{d}(\bar{d}_{\mathrm{Ni}}))/\mathrm{d}t$ on $\bar{d}_{\mathrm{Ni}}$ as obtained here, which gives confidence to the equation derived above for $(\mathrm{d}(\bar{d}_{\mathrm{Ni}}))/\mathrm{d}t$, Eq. (21), and the ability of this equation to predict the effect of nickel loading, the carrier surface area, and the temperature.

Before comparing model predictions with experimental data, Eq. (21) is integrated and an expression for the nickel

surface area is derived:

$$\bar{d}_{\mathrm{Ni}}^{7} - \bar{d}_{\mathrm{Ni},0}^{7} = \text{const.}\frac{D_{\mathrm{Ni}} X_{\mathrm{Ni}} t}{(1 - X_{\mathrm{Ni}}) A_{\mathrm{car}}} K_1. \tag{22}$$

From this equation $\bar{d}_{\mathrm{Ni}}$ can be isolated:

$$\bar{d}_{\mathrm{Ni}} = \left(\text{const.}\frac{K_1 D_{\mathrm{Ni}} X_{\mathrm{Ni}} t}{(1 - X_{\mathrm{Ni}}) A_{\mathrm{car}}} + \bar{d}_{\mathrm{Ni},0}^{7}\right)^{1/7}, \tag{23}$$

$$\bar{d}_{\mathrm{Ni}} \approx \text{const.}\frac{K_1^{0.14} D_{\mathrm{Ni}}^{0.14} X_{\mathrm{Ni}}^{0.14} t^{0.14}}{(1 - X_{\mathrm{Ni}})^{0.14} A_{\mathrm{car}}^{0.14}}. \tag{24}$$

Expression (24) is a good approximation for Eq. (23) when the averaged nickel particle diameter is increased by more than 40% compared to that of the fresh catalyst. In this case, $\text{const.}(K_1^{0.14} D_{\mathrm{Ni}}^{0.14} X_{\mathrm{Ni}}^{0.14} t^{0.14})/((1 - X_{\mathrm{Ni}})^{0.14} A_{\mathrm{car}}^{0.14}) = 9.5\bar{d}_{\mathrm{Ni},0}$. If the increase in $\bar{d}_{\mathrm{Ni}}$ compared to the initial stage is less than that, weaker dependencies of $\bar{d}_{\mathrm{Ni}}$ on X_{Ni}, A_{car}, and t will be found. From Eq. (24) an equation for the nickel surface area can be derived:

$$\begin{aligned} A_{\mathrm{Ni}} &= \pi c_{\mathrm{cat}} \bar{d}_{\mathrm{Ni}}^{2} = \text{const.} X_{\mathrm{Ni}} \bar{d}_{\mathrm{Ni}}^{-1} \\ &\approx \text{const.}\frac{X_{\mathrm{Ni}}^{0.86} (1 - X_{\mathrm{Ni}})^{0.14} A_{\mathrm{car}}^{0.14}}{K_1^{0.14} D_{\mathrm{Ni}}^{0.14} t^{0.14}}. \end{aligned} \tag{25}$$

4.6. Discussion of the model and comparison with experimental data

The equations above are now explored and it is discussed how they correspond to the experimental data obtained here and to literature data on sintering of metal particles on ceramic supports. Several interesting features arise from this simple model.

First, the time dependence of the nickel surface area is discussed. The nickel surface area is proportional to the time in the order of -0.14 in Eq. (25). Most of the data in the literature were analyzed using the power-law expression given previously,

$$-\frac{\mathrm{d}A_{\mathrm{Ni}}}{\mathrm{d}t} = k A_{\mathrm{Ni}}^{n}, \tag{1}$$

and values of n are reported. A reaction order for the time of -0.14 corresponds to $n = 8$. The values reported for n in the literature can be obtained from the review of Bartholomew [7]. For supported nickel catalysts, values of n in the range 3–15 with an average of 8.6 have been reported and for supported platinum catalysts, values of 2–14 with an average of 7.2 were given. These values are close to the value of 8 predicted by Eq. (25). One explanation for the high values of n could be that faceting of the metal particles may retard the sintering process and lead to higher values of n [22]. As discussed in previous work, large nickel particles show facetting [10]. Another explanation for the high values of n could be that the initial metal particle-size distributions of the freshly prepared catalysts are narrow leading to fast initial sintering followed by a plateau of slower sintering when lognormal particle distributions have been reached. In this case, a fit of Eq. (1) to the experimental data will result in very high values of n. A third reason for the experimentally observed high values of n could be the effects of the carrier. Certain particle sizes may fit into the cavities in the carrier, thereby lowering the surface energies [31–33], which may increase the values of n in some situations.

Low values of n are normally observed for sintering at high temperatures and are normally accompanied by changes in the particle-size distributions to non-lognormal distributions. This is attributed to a change in the sintering mechanism from particle migration and coalescence at low temperatures to atom migration (Ostwald Ripening) at high temperatures as discussed previously.

The dependencies of the nickel surface area on the nickel loading, the carrier surface area, and the temperature are now examined. According to Eq. (25), the nickel surface area is proportional to $A_{\mathrm{car}}^{0.14} X_{\mathrm{Ni}}^{0.86} (1 - X_{\mathrm{Ni}})^{0.14}$. The dependence of the nickel surface area on the surface area of the carrier is given in Fig. 2. It is shown in Fig. 2 that A_{Ni} is proportional to $A_{\mathrm{car}}^{0.3\pm0.1}$, which is close to the dependence predicted by Eq. (25) of $A_{\mathrm{car}}^{0.14}$. This surprisingly weak dependence of A_{Ni} on A_{car} can therefore be rationalized theoretically. The reason for the stronger dependence of A_{Ni} on A_{car} observed experimentally compared to that obtained theoretically may be that some particles are trapped in cavities in the carrier with high surface area.

The effect of the nickel loading on A_{Ni} predicted by Eq. (25) is also in good agreement with experimental data. In Fig. 1, the predictions of the nickel surface area of the catalysts supported on 15 and 50 $\mathrm{m^2\,g^{-1}}$ are plotted as a function of X_{Ni}. As seen from the figure, the fitted trends in the stable sulfur capacity are in very good agreement with the observed trends. The reason for the relatively strong dependence of the nickel surface area on the nickel loading and the weak dependence on the surface area of the carrier can be understood physically as follows. The mobility of the nickel particles is strongly dependent on the diameter of the nickel particles. Eq. (13) predicts that the average collision probability per gram depends on $\bar{d}_{\mathrm{Ni}}^{-6}$ and linearly on the diffusion coefficient of the nickel particles. Eq. (18) shows that for spherical particles, the diffusion coefficient of nickel particles depends on the average nickel particle diameter in the power of -4. Increasing the surface area of the carrier or decreasing the nickel loading increases the average distance between the nickel particles. However, since the mobility of the particles depends strongly on the particle size, the increase in the distance between the particles will only result in a small reduction of the nickel particle size after sintering. Only a small increase in the particle size is necessary to decrease the mobility of the particles so much that it compensates for the decreased distance between the particles. In conclusion, the strong effect on A_{Ni} of the nickel loading and the weak effect of the carrier surface area are a consequence of the strong dependence of the mobility of the particles on the particle diameter. Obviously, a limit that depends on the surface area of the carrier exists at very high nickel loadings,

where the nickel particles are so close that they are almost touching each other. In this case, the nickel surface area no longer increases with the nickel loading.

The temperature dependence of the nickel surface area obtained from Eq. (25) is determined by the activation energy for diffusion on a nickel atom at the nickel surface, i.e., the temperature dependence of D_{Ni} and the energy of formation of a transport species at the surface of the nickel particles. In Fig. 3 the nickel surface areas of a nickel catalyst supported on 24 $m^2\,g^{-1}$ $MgAl_2O_4$ obtained after 700 h of sintering in a gas mixture containing $H_2O{:}H_2 = 10{:}1$, 30 bar total pressure, and a temperature of 520–682 °C are plotted. When analyzed by an Arrhenius expression [Eq. (3)], the apparent Arrhenius energy derived from the nickel surface areas is $-(46 \pm 8)$ kJ/mol. The negative value shows that the nickel surface area is lower at higher temperatures as observed.

Values of the diffusion coefficient of nickel add-atoms over nickel planes, along edges and kinks and descending from a step at a nickel surface, and an ascending motion of edge nickel atoms have been reported [38–41]. Calculations show that the barrier for add-atom migration is lower than diffusion of surface vacancies [38]. The activation energies of diffusion are within 5–200 kJ/mol [38–41]. However, as discussed previously, the barrier toward formation of the surface transport species as add-atoms is high—of the order of 111 kJ/mol [28]. This barrier must be included in the expression of the effective diffusion constant for particle diffusion.

For add-atoms the lowest diffusion barrier is observed for the diffusion over Ni(111). The highest barriers were determined at very high temperatures to be up to 200 kJ/mol [38], which is not really relevant for this study. However, the interesting barrier is the barrier for the slowest step in the transport process at the surface of the nickel particles. This is presumably the transport process with the highest barrier. Liu and Adams [40] calculated a barrier of 129 kJ/mol for diffusion of a nickel atom from a terrace down to a ledge at a Ni(110) surface. Since nickel particles also have to expose facets with higher surface energy than Ni(111) in order to get the lowest possible total energy [42], some of the nickel atoms on the surface of the nickel particle presumably have to overcome the barrier of 129 kJ/mol. In Eq. (25), the temperature dependence of A_{Ni} for spherical particles is given by $(K_1 D_{\mathrm{Ni}})^{-0.143}$. Using an activation energy for diffusion of 129 kJ/mol and an energy of formation of an add-atom of 111 kJ/mol, an Arrhenius energy for A_{Ni} of $-0.143(111+129)$ kJ/mol $= -34$ kJ/mol is obtained. Considering the uncertainty in this estimate there is a reasonable agreement with the $-(46 \pm 8)$ kJ/mol determined experimentally.

Finally, we analyze the average particle diameters calculated from the active surface areas reported by Rasmussen et al. [13] for an alumina-supported nickel catalyst sintered at ambient pressure using $H_2O{:}H_2 = 1{:}1$. The relative surface-averaged nickel particle diameters obtained by sulfur chemisorption and Eq. (2) are plotted with filled symbols

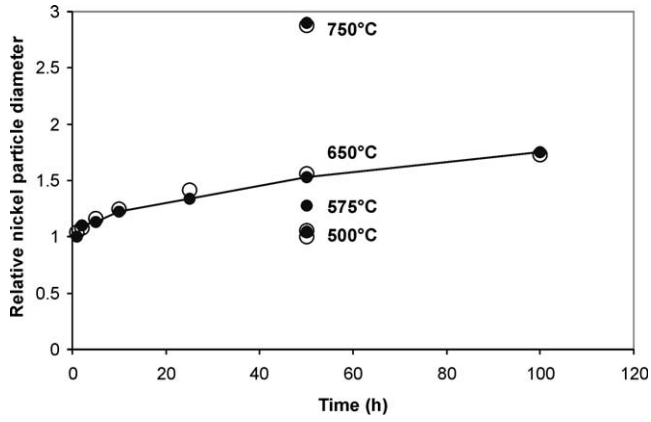

Fig. 4. Relative nickel particle diameters obtained from sulfur chemisorption plotted as a function of the sintering time (filled symbols). The data were taken from Rasmussen et al. [13]. The sintering was performed at ambient pressure and $H_2O{:}H_2 = 1{:}1$. Four sintering temperatures were used: 500, 575, 650, and 750 °C. Lines are connecting the data obtained using a temperature of 650 °C and the open symbols represent a fit to the experimental data. See text for details.

in Fig. 4. The data point obtained after sintering at 825 °C is excluded from the figure because another sintering mechanism is expected to be activated at this temperature [13]. A modification of Eq. (23) was fitted to the data in Fig. 4:

$$\frac{\bar{d}_{\mathrm{Ni}}}{\bar{d}_{\mathrm{Ni},0}} = \left(\frac{\text{const.}}{A_{\mathrm{car}}} \mathrm{e}^{-E_a/RT} t + 1\right)^{1/7}. \tag{26}$$

The two fitted parameters are const. and E_a and the fitted data points are given as open symbols in Fig. 4. The BET areas per gram of carrier ($m^2\,g^{-1}$) were used as values for A_{car} in the fit. As seen from the figure, the fit to the data is good. The obtained constants are const. $= \exp(47.18)$ $m^2\,g^{-1}\,h^{-1}$ and $E_a = 332$ kJ/mol. $0.143 E_a = 47$ kJ/mol should be compared with the apparent Arrhenius energy of the plot in Fig. 3. There is good agreement between the apparent Arrhenius energy obtained from Fig. 4 ($E_a = 47$ kJ/mol) and the one determined from the data in Fig. 3 ($E_a = 46$ kJ/mol) as well as the one derived by the theoretical considerations ($E_a \approx 34$ kJ/mol) presented above.

5. Conclusions

The sintering of eight nickel steam-reforming catalysts were studied under conditions similar to those used in an industrial reformer, i.e., in an atmosphere of $H_2O{:}H_2 = 10{:}1$ at 500 °C and 30 bar total pressure. Additional experiments were performed with a single reforming catalyst under simulated, industrial steam-reforming conditions, i.e., in a mixture of steam and hydrogen (10:1) in the temperature range 520–682 °C, and at 30 bar total pressure. The data were analyzed using a simple model for the nickel surface area derived assuming particle migration and coalescence as the rate-determining step and lognormal particle size distributions and only weak interactions with the carrier. The

dependence of the nickel surface area on the sintering time, the nickel loading, the carrier surface area, and the temperature is predicted correctly by the model. The model increases our fundamental understanding of the sintering phenomena but also provides a tool for predictions of metal surface areas of used supported catalysts.

Acknowledgments

Thanks are due to Erik H. Christensen, Ulla Ebert, Jakob S. Jensen, and Henning Kosack for their technical assistance, to Joachim Jacobsen for suggestions and discussions of the manuscript, and to Jens K. Nørskov for general discussions of catalyst sintering.

References

[1] J.R. Rostrup-Nielsen, in: J.R. Anderson, M. Boudart (Eds.), Catalysis, Science and Technology, Vol. 5, Springer, Berlin, 1984, Chap. 1.
[2] J.R. Rostrup-Nielsen, J. Sehested, J.K. Nørskov, Adv. Catal. 47 (2002) 65.
[3] J.T. Richardson, J.G. Crump, J. Catal. 57 (1979) 417.
[4] A. Teixeira, R. Giudici, Chem. Eng. Sci. 54 (1999) 3609.
[5] H.K. Kuo, P. Ganesan, R.J. Deangelis, J. Catal. 64 (1980) 303.
[6] C.H. Bartholomew, W.L. Sorensen, J. Catal. 81 (1983) 131.
[7] C.H. Bartholomew, Appl. Catal. A 107 (1993) 1.
[8] D.J. Young, P. Udaja, D.L. Trimm, Surf. Sci. Catal. 6 (1980) 331.
[9] M.S. Borisova, V.B. Fenelov, V.A. Dzisko, L.G. Simonova, Kinet. Katal. 17 (1976) 653.
[10] J. Sehested, A. Carlson, T.V.W. Janssens, P.L. Hansen, A.K. Datye, J. Catal. 197 (2001) 200.
[11] J.T. Richardson, J.L. Propp, J. Catal. 98 (1986) 457.
[12] Å. Slagtern, U. Olsbye, R. Blom, I.M. Dahl, H. Fjellvåg, Appl. Catal. A 165 (1997) 379.
[13] F.B. Rasmussen, J. Sehested, H.T. Teunissen, A.M. Molenbroek, B.S. Clausen, J. Phys. Chem. (2002), Submitted.
[14] I. Chen, F. Chen, Ind. Eng. Chem. Res. 29 (1990) 534.
[15] ASTM D4567, Standard Test Method for Single-Point Determination of Specific Surface Area of Catalysts Using Nitrogen Adsorption by Continuous Flow Method.
[16] I. Alstrup, J.R. Rostrup-Nielsen, S. Røen, Appl. Catal. 1 (1981) 303.
[17] C.G. Granqvist, R.A. Buhrman, Appl. Phys. Lett. 27 (1975) 693.
[18] C.G. Granqvist, R.A. Buhrman, J. Catal. 46 (1977) 238.
[19] C.G. Granqvist, R.A. Buhrman, J. Catal. 42 (1976) 477.
[20] C.G. Granqvist, R.A. Buhrman, J. Appl. Phys. 47 (1976) 2200.
[21] S.E. Wanke, J. Catal. 46 (1977) 234.
[22] P. Wynblatt, N.A. Gjostein, Prog. Solid State Chem. 9 (1975) 21.
[23] Y. De Smet, L. Deriemaeker, R. Finsy, Langmuir 13 (1997) 6884.
[24] G.A. Fuentes, E. Salinas-Rodriguez, Stud. Surf. Sci. 139 (2001) 503.
[25] R. Hughes, Deactivation of Catalysts, Academic Press, London, 1984.
[26] T.W. Hansen, J.B. Wagner, P.L. Hansen, S. Dahl, H. Topsøe, C.J.H. Jacobsen, Science 294 (2001) 1508.
[27] I. Barin, Thermodynamic Data of Pure Substances, VCH, Weinheim, 1989.
[28] H.S. Bengaard, PhD thesis, 2002.
[29] M. Humenik, W.D. Kingery, J. Am. Ceram. Soc. 37 (1954) 18.
[30] P.L. Hansen, J.B. Wagner, S. Helveg, J.R. Rostrup-Nielsen, B.S. Clausen, H. Topsøe, Science 295 (2002) 2053.
[31] E. Ruckenstein, B. Pulvermacher, J. Catal. 37 (1975) 416.
[32] T.-M. Ahn, J.K. Tien, P. Wynblatt, J. Catal. 66 (1980) 335.
[33] E. Stassinos, H.H. Lee, Chem. Eng. Sci. 50 (1995) 1337.
[34] E. Ruckenstein, B. Pulvermacher, AIChE J. 19 (1973) 356.
[35] S. Chandrasekhar, Rev. Mod. Phys. 15 (1943) 1.
[36] E.E. Gruber, J. Appl. Phys. 38 (1967) 243.
[37] P.K. Handa, J.C. Matthews, AIChE J. 29 (1983) 717.
[38] R.T. Tung, W.R. Graham, Surf. Sci. 97 (1980) 73.
[39] C.-L. Liu, J.M. Cohen, J.B. Adams, A.F. Voter, Surf. Sci. 253 (1991) 334.
[40] C.-L. Liu, J.B. Adams, Surf. Sci. 265 (1992) 262.
[41] T.-Y. Fu, T.T. Tsong, Surf. Sci. 454-456 (2000) 571.
[42] R. Van Hardeveld, F. Hartog, Surf. Sci. 15 (1969) 189.